ACS APPLIED MATERIALS & INTERFACES

Research Article

www.acsami.org

Size and Aging Effects on Antimicrobial Efficiency of Silver Nanoparticles Coated on Polyamide Fabrics Activated by Atmospheric DBD Plasma

Andrea Zille,*[,†] Margarida M. Fernandes,[‡] Antonio Francesko,[‡] Tzanko Tzanov,[‡] Marta Fernandes,[†] Fernando R. Oliveira,[§] Luís Almeida,[†] Teresa Amorim,[†] Noémia Carneiro,[†] Maria F. Esteves,[†] and António P. Souto[†]

[†]Centro de Ciência e Tecnologia Têxtil (2C2T), Universidade do Minho, Campus de Azurém, 4800-058 Guimarães, Portugal

[‡]Group of Molecular and Industrial Biotechnology, Department of Chemical Engineering, Universitat Politècnica de Catalunya, Rambla Sant Nebridi, 22, 08222 Terrassa, Spain

[§]Department of Textile Engineering, Federal University of Rio Grande do Norte, Av. Salgado Filho, 3000, Lagoa Nova, Natal, RN, 59078-970 Brazil

Supporting Information

ABSTRACT: This work studies the surface characteristics, antimicrobial activity, and aging effect of plasma-pretreated polyamide 6,6 (PA66) fabrics coated with silver nanoparticles (AgNPs), aiming to identify the optimum size of nanosilver exhibiting antibacterial properties suitable for the manufacture of hospital textiles. The release of bactericidal Ag^+ ions from a 10, 20, 40, 60, and 100 nm AgNPs-coated PA66 surface was a function of the particles' size, number, and aging. Plasma pretreatment promoted both ionic and covalent interactions between AgNPs and the formed oxygen species on the fibers, favoring the deposition of smaller-diameter AgNPs that consequently showed better immediate and durable antimicrobial effects against Gram-negative *Escherichia coli* and Gram-positive *Staphylococcus aureus* bacteria. Surprisingly, after 30 days of aging, a comparable bacterial growth inhibition was achieved for all of the fibers treated with AgNPs <100 nm in size. The Ag^+ in the coatings also favored the electrostatic stabilization of the plasma-induced functional groups on the PA66 surface, thereby retarding the aging process. At the same time, the size-related ratio (Ag^+/Ag^0) of the AgNPs between 40 and 60 nm allowed for the controlled release of Ag^+ rather than bulk silver. Overall, the results suggest that instead of reducing the size of the AgNPs, which is associated with higher toxicity, similar long-term effects can be achieved with larger NPs (40−60 nm), even in lower concentrations. Because the antimicrobial efficiency of AgNPs larger than 30 nm is mainly ruled by the release of Ag^+ over time and not by the size and number of the AgNPs, this parameter is crucial for the development of efficient antimicrobial coatings on plasma-treated surfaces and contributes to the safety and durability of clothing used in clinical settings.

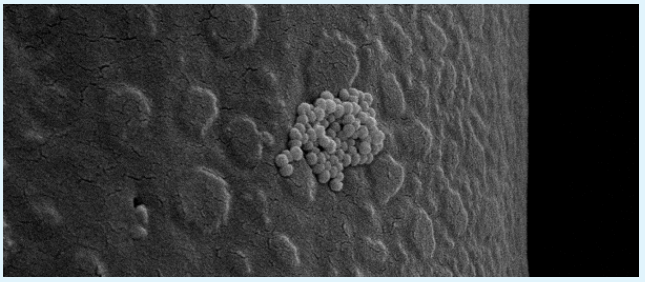

KEYWORDS: *dielectric barrier discharge plasma, polyamide fabric, silver nanoparticles, antimicrobial effect, aging*

1. INTRODUCTION

Nowadays, the increasing resistance of pathogenic bacteria to conventional antibiotics requires new efficient, nontoxic, durable, and cost-effective antimicrobial agents.[1] Bactericidal silver has emerged as a viable option because it induces far less propensity for resistance mutations compared to antibiotics.[2] Silver ions kill bacteria in a multitargeted mechanism of action by binding to and disrupting bacterial cell walls, damaging intracellular and nuclear membranes, poisoning respiratory enzymes, and denaturing bacterial DNA and RNA.[3] In addition, silver processed at the nanoscale level provides better contact between the material and a broad range of microorganisms due to the high surface energy, enhanced physicochemical and biological properties, and extremely large surface area.[4] Nanosilver is currently being exploited in wound dressings, cosmetic lotions, dental materials, antimicrobial textiles, and for wastewater treatment, among other uses.[1]

However, in the last few years, concerns about the release and fate of silver into the environment have been raised.[5] Moreover, the use of environmentally hazardous surfactants and reducing agents to synthesize silver nanoparticles (AgNPs) as well as the toxic chemicals used for the nanoparticle (NP) deposition onto various surfaces limits their applications in the medical field.[6] Therefore, the development of biocompatible

Received: November 19, 2014
Accepted: June 9, 2015
Published: June 9, 2015

DOI: 10.1021/acsami.5b04340
ACS Appl. Mater. Interfaces 2015, 7, 13731−13744

and eco-friendly methods for NP deposition becomes one of the most important topics in nanotechnology research for antimicrobial textiles today.[7] In this context, atmospheric plasma is an alternative that is cost-competitive to the wet chemical treatment method. The use of plasma as a pretreatment for NP deposition avoids the need for toxic solvents and expensive vacuum equipment while still allowing continuous and uniform processing of the material.[8] Among the atmospheric plasma technologies, dielectric barrier discharge (DBD) technology is one of the most effective for surface preactivation of polymers before their coating with AgNPs for medical uses.[9] Nevertheless, the plasma treatment of polymers has one major drawback: the induced modification of the surface is not permanent, and after a period of time the surface tends to recover its original state (aging) due to the migration and diffusion of short-chain oxidized molecules and functional groups into the polymer bulk.[10]

Despite the knowledge on the aging phenomenon, very little information is available about the durability and antimicrobial efficacy over time of AgNPs deposited onto plasma-treated surfaces. It is known that the size, shape, and crystalline structure of AgNPs affect to a certain extent their bactericidal effect, but their antimicrobial efficacy truly depends on the dissolution rate and concentration of silver ions on the particle surface.[11,12] Most of the available data for silver antibacterial efficiency are, however, obtained for NPs in suspension, while the mechanism of bactericidal action of deposited AgNPs largely remains unknown due to the complexity of the heterogeneous interactions between the immobilized particles and the living organisms.[13,14] There are also no reports on the size-dependent antimicrobial activity and durability of AgNPs deposited on plasma-functionalized polymers. Additionally, recent health concerns are related to the increased use of biomedical devices incorporating AgNPs smaller than 30 nm that easily penetrate the human skin.[15]

This study develops and optimizes the coating of PA66 fabrics with nanosilver, targeting the production of durable antibacterial textiles with an aim to prevent the spread of nosocomial infections in clinical settings. Because textiles are prone to microbial contaminations, their coating with durable antimicrobial finishes impedes both the person-to-person transmission of pathogens in hospitals and the acquired infection incidence. The herein described strategy is in line with the global need to reduce the occurrence of hospital infections through the sustainable manufacture of antimicrobial hospital clothing, e.g., doctors' aprons, gowns, patients' pajamas, bed sheets, curtains, etc. Different aspects of investigation on the nanosilver-coated PA66 are covered, namely: (i) the physicochemical binding mechanism over time between different-sized AgNPs and DBD-plasma treated fabric; (ii) the relation between the size and antimicrobial efficacy of the coated AgNPs, and (iii) the durability of such effect in terms of aging and resistance to washings. To this end, we employed five commercial AgNPs with sizes of 10, 20, 40, 60, and 100 nm for the fabrics coating. The particles were deposited on plasma-treated polyamides and their properties analyzed after 30 days of aging and after applying different number of washing cycles (up to 20). Fourier transform infrared attenuated total reflection (FTIR-ATR), UV−vis, and reflectance spectroscopies, static and dynamic contact angle measurements, scanning electron microscopy (SEM), energy dispersive X-ray spectroscopy (EDS), and and X-ray photoelectron spectroscopy (XPS) were used to characterize the fabrics and the deposited AgNPs. The antimicrobial effect of the obtained materials was evaluated against the medically relevant strains *Staphylococcus aureus* and *Escherichia coli*.

2. EXPERIMENTAL SECTION

2.1. Materials. Commercial PA66 fabric with a warp density of 40 threads cm^{-1}, a weft density of 18 threads cm^{-1}, and weight per unit area of 135 g m^{-2} was used in this study. The samples were prewashed with 1% nonionic detergent at 30 °C for 30 min, rinsed with water for another 15 min, and finally dried before DBD plasma treatment. Aqueous dispersions of 0.02 g L^{-1} AgNPs with sizes of 10, 20, 40, 60, and 100 nm were provided by Sigma-Aldrich. All other reagents were analytical grade, purchased from Sigma-Aldrich, and used without further purification.

2.2. Plasma Treatment. The DBD plasma treatment was conducted in a semi-industrial prototype (Softal Electronics GmbH and University of Minho), working at room temperature and atmospheric pressure, using a system of metal electrodes coated with ceramic and counter electrodes coated with silicon, with a 50 cm effective width, a gap distance fixed at 3 mm, and producing the discharge at high voltage (10 kV) and low frequency (40 kHz). A total of five different discharge dosages (0.5, 1, 2, 2.5, and 3.5 kW min m^{-2}) were tested to optimize the plasmatic effect onto the fabric surface. The machine was operated with optimized parameters: 1 kW power, 4 m min^{-1} velocity, and five passages corresponding to a dosage of 2.5 kW min m^{-2}. The plasmatic dosage was defined by eq 1:

$$\text{Dosage} = \frac{N \cdot P}{v \cdot l} \tag{1}$$

where N is the number of passages, P is the power (W), v is the velocity (m min^{-1}), and l is the width of treatment (0.5 m).

2.3. Silver Nanoparticle Deposition on Polyamide. Untreated and DBD-plasma-treated PA66 fabrics (0.1 g per sample) were immersed in 2 mL of a 0.02 g L^{-1} silver nanoparticle dispersion (10, 20, 40, 60, and 100 nm particle size) in aqueous buffer containing sodium citrate as stabilizer under 200 rpm orbital shaking using a sterile six-well cell culture plate for 15 min. Thereafter, all samples were cured at 100 °C for 5 min to eliminate the residual condensation between the textile and the nanoparticles. The samples were then rinsed with deionized water and dried at room temperature. The entire procedure was repeated twice. A total of two controls were used: a pristine control (Cp) and a processed control (Ct) that followed the same procedure of nanoparticle deposition (pad−dry−cure) as describe above but without AgNPs. All measurements were performed in triplicate. All samples were aged 30 days at relative humidity (60 ± 10%) and 25 °C under the natural photoperiod.

2.4. Scanning Electron Microscopy and Energy Dispersive X-ray Spectroscopy. Morphological analyses of nanofibers were carried out with an ultrahigh-resolution field emission gun scanning electron microscope (FEG-SEM), a NOVA 200 Nano SEM (FEI Company). Secondary electron images were acquired with an acceleration voltage of 5 kV. Backscattering electron images were realized with an acceleration voltage of 15 kV. Samples were covered with a film of Au−Pd (80−20 wt %) in a high-resolution sputter coater (208HR Cressington Company) coupled to a MTM-20 Cressington high-resolution thickness controller. The atomic compositions of the membrane were examined with the EDS capability of the SEM equipment using an EDAX Si(Li) detector and an acceleration voltage of 5 kV. Prior SEM analysis silver-loaded plasma-treated PA66 samples were rinsed twice in 100 mL of deionized water for 10 min.

2.5. Spectrophotometric Measurements. UV−vis spectroscopy (Shimadzu UV-1800 spectrophotometer) was used to evaluate the stability of the colloidal silver dispersion over the experimental period. Each sample was diluted twice before measurement to maintain the concentration in the linear zone. A total of five dilutions of the initial concentration (0.02 mg mL^{-1}) were prepared for each nanoparticle size using distilled water. The absorbance at the maximum wavelength of each nanoparticle size was recorded and plotted versus the concentration of the solution. The extinction coefficient was obtained

DOI: 10.1021/acsami.5b04340
ACS Appl. Mater. Interfaces 2015, 7, 13731−13744

from the slope of the linear region of the absorbance−concentration curve according to the Lambert−Beer law. The diffuse reflectance of the PA66 fabrics that were untreated and plasma-treated with adsorbed AgNPs were measured using a Spectraflash 600 (Datacolor) spectrophotometer at the standard illuminant D65 (LAV/specular excluded, d/8, D65/10°). All measurements were performed in triplicate. The data were expressed as the percentage of reflectance decrease after AgNPs loading in the nanoparticles' maximum wavelength absorbance with respect to the untreated and plasma-treated PA66 controls.

2.6. Contact Angle and Surface Free Energy Measurement. The water surface wettability of PA66 fabrics untreated and treated with plasma, without and with silver nanoparticles, was characterized by static and dynamic contact angle measurements (based on the sessile drop principle) made with Dataphysics equipment (Filderstadt, Germany) using OCA20 software with a video system to capture images in static and dynamic modes. All the measurements were performed immediately and after 30 days of the plasmatic and AgNP deposition treatment to evaluate the aging effect. All the experiments were replicated five times, and the data are reported as mean ± standard deviation. For the calculation of the surface energy, three liquids with known surface energies (γ) were used: distilled water (γ 72.8, γ^D 29.1, γ^P 43.7), PEG 200 (γ 43.5, γ^D 29.9, γ^P 13.6), and glycerol (γ 63.4, γ^D 37.4, γ^P 26.0). The surface energy was considered to be composed of polar and dispersive components. In particular, the polar component results from three different intermolecular forces were due to permanent and induced dipoles and hydrogen bonding, whereas the dispersion (nonpolar) component of γ is due to instantaneous dipole moments. The work of adhesion (W_{Adh}), which represents the energy of interaction between the liquid and the solid phases per unit area, was defined by eq 2.

$$W_{Adh} = \gamma_l(1 + \cos\theta) \tag{2}$$

where θ is the water contact angle calculated by goniometer, and γ_l means the "liquid" surface energy. For polar solids or liquids, the total γ, defined by eq 3, is a sum of the always-existing London dispersion forces (γ^D) with intermolecular interactions that depend on the chemical nature of the material, compiled as polar forces (γ^P):

$$\gamma = \gamma^D + \gamma^P \tag{3}$$

The polar and dispersive components of the surface energy (γ^D and γ^P, respectively) were calculated with the Wu method (harmonic mean) by eq 4:

$$\gamma_{sl} = \gamma_s + \gamma_l - 4\left[\frac{\gamma_s^D\gamma_l^D}{\gamma_s^D + \gamma_l^D} + \frac{\gamma_s^P\gamma_l^P}{\gamma_s^P + \gamma_l^P}\right] \tag{4}$$

2.7. X-ray Photoelectron Spectroscopy. Analyses using x-ray photoelectron spectroscopy (XPS) were performed using a Kratos AXIS Ultra HSA with VISION software for data acquisition and CASAXPS software for data analysis. The analysis was carried out with a monochromatic Al Kα X-ray source (1486.7 eV) operating at 15 kV (150 W) in fixed analyzer transmission (FAT) mode with a pass energy of 40 eV for regions ROI and 80 eV for survey. Data acquisition was performed with a pressure lower than 1×10^{-6} Pa, and it was used a charge neutralization system. Spectra have been charge-corrected to give the adventitious C 1s spectral component (C−C, C−H) a binding energy of 285 eV. High-resolution spectra were collected using an analysis area of ≈1 mm^2. The peaks were constrained to have an equal full width half maximum to the main peak. This process has an associated error of ±0.1 eV. Spectra were analyzed for elemental composition using CasaXPS software (version 2.3.15). Deconvolution into subpeaks was performed by least-squares peak analysis software, XPSPEAK version 4.1, using the Gaussian/Lorenzian sum function and Shirley-type background subtraction. No tailing function was considered in the peak fitting procedure. The components of the various spectra were mainly modeled as symmetrical Gaussian peaks unless a certain degree of Lorentzian shape was necessary for the best fit. The best mixture of Gaussian−Lorentzian components was defined based on the instrument and resolution (pass energy) settings used, as well as the natural line width of the specific core hole.

The reduced χ^2 is the sum of the squares of the difference between the experimental spectrum and the fitted envelope at each point over the peak region of interest, divided by the variance. A reduced χ^2 value of less than or equal to 2 is typically regarded as indicative of an acceptable peak-fit. Values for χ^2 between 0.1 and 0.7 were obtained for all the peak fittings in C, O, and N high-resolution spectra demonstrating a good fit quality. With the exception of the 10 nm AgNPs (χ^2 of 0.1), the deconvoluted Ag spectra showed a χ^2 between 3.5 and 4.5, indicating a limited optimization of the fitting but no missing signals from the peak fitting (Table S4 in the Supporting Information).[16]

In XPS analysis, the estimated atomic composition error is based on the detection limit of the system and the uncertain propagation. In this work, where comparison between samples is the preferred approach, the systematic error is very similar among samples and the random error arising from the Poisson statistics of electron detection. The three survey spectra (80 eV) and the high-resolution spectrum (40 eV) for each sample performed in this work are capable of providing sufficient precision in the quantified elemental compositions so that the comparison can be made with statistical confidence. Photoelectron peak area counts that were larger than that of the background by at least two times the background noise (not intensities) were used for quantitative analysis.

Because it is easier to detect trace heavy elements in a light element matrix, the detection limit for Ag in the polyamide carbon matrix was estimated as 0.01 At % (atomic percent) by the Shard's method using the intensity of the background at the expected position for the photoelectron peak to be detected.[17]

2.8. FTIR-Attenuated Total Reflection Spectroscopy. A Nicolet Avatar 360 FTIR spectrophotometer (Madison, WI, USA) with an attenuated total reflectance (ATR) accessory was used to record the FTIR-ATR spectra of the fabrics, performing 60 scans at a spectral resolution of 16 cm^{-1} over the 650−4000 cm^{-1} range. All measurements were performed in triplicate immediately and after 30 days of the plasmatic and AgNP deposition to evaluate the aging effect.

2.9. Antimicrobial Assay. The antimicrobial activity was assessed according to the standard shake flask method (ASTM-E2149-01). This method provides quantitative data for measuring the reduction rate in number of colonies formed, converted to the average colony-forming units per milliliter of buffer solution in the flask (CFU mL^{-1}). For preparation of *Escherichia coli* (*E. coli*) and *Staphylococcus aureus* (*S. aureus*) inoculum, a single colony from the corresponding stock bacterial cultures was used. The culture was then inoculated overnight in sterile nutrient broth (NB, Sharlab, Spain) at 37 °C and 230 rpm. The inoculated bacterial culture was harvested by centrifugation and washed twice with a 0.9% solution of NaCl at pH 6.5. The absorbance of the solution was adjusted to 0.28 ± 0.01 for *E. coli* and to 0.36 ± 0.01 for *S. aureus* at 600 nm, which corresponds to 1.5−3.0 × 10^8 CFU mL^{-1}. Thereafter, the PA66 fabrics (0.05 g) were incubated with 5 mL of bacterial suspension (previously diluted 10-fold with NaCl 0.9% at pH 6.5) at 37 °C and 100 rpm. For determination of the inoculum cell density, the suspensions were withdrawn before contact with the fabrics and after 2 h of contact. The withdrawn suspensions were serially diluted in sterile buffer solution, plated on plate count agar, and further incubated at 37 °C for 24 h to determine the number of surviving bacteria. Antimicrobial activity, defined by eq 5, is reported in terms of the percentage of bacteria reduction, calculated as the ratio between the number of surviving bacteria after and before the contact with the coated fabrics:

$$\text{bacteria reduction (\%)} = \left[\frac{A - B}{A}\right] \times 100 \tag{5}$$

where A and B are the average number of bacteria before and after the contact with the samples, respectively. The durability of the antibacterial properties was also evaluated using the same method on the PA66 treated with 40 nm AgNPs (with and without plasma). To this end, we washed the samples 1, 5, 10, and 20 times using the

DOI: 10.1021/acsami.5b04340
ACS Appl. Mater. Interfaces 2015, 7, 13731−13744

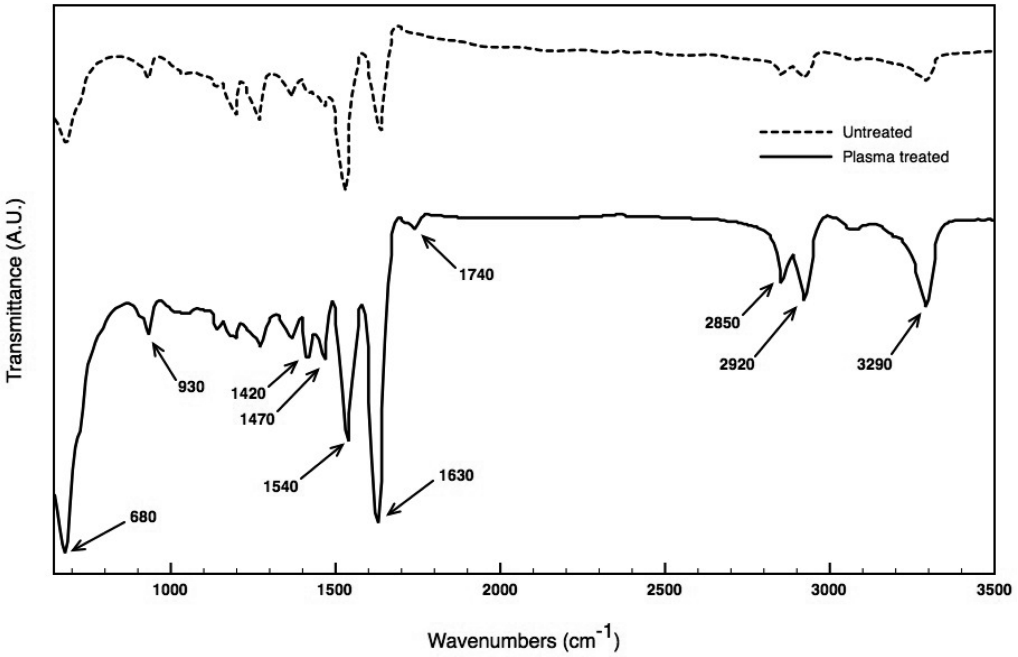

Figure 1. FTIR-ATR spectra of PA66 fabric with (solid line) and without (dashed line) plasma treatment.

Table 1. Relative Chemical Composition and Atomic Ratios of Untreated and DBD Plasma-Treated PA66 Fabrics at Day 1 and After 30 Days Coated with 10 and 100 nm AgNPs[a]

		untreated						plasma-treated					
		chemical composition (%)				atomic ratio		chemical composition (%)				atomic ratio	
		C 1s	N 1s	O 1s	Ag 3d	O/C	N/C	C 1s	N 1s	O 1s	Ag 3d	O/C	N/C
day 1	Cp	74.25	9.38	16.37	ND	0.22	0.13	62.75	10.28	26.97	ND	0.43	0.16
	Ct	79.24	7.59	13.17	ND	0.17	0.10	75.90	9.43	14.67	ND	0.19	0.12
	10 nm	78.30	8.20	13.48	0.03	0.17	0.10	75.51	9.26	14.78	0.45	0.20	0.12
	100 nm	78.14	8.34	13.52	ND	0.17	0.11	76.78	9.17	14.03	0.03	0.18	0.12
day 30	Cp	74.67	7.58	17.75	ND	0.24	0.10	70.25	9.92	19.83	ND	0.28	0.14
	Ct	79.21	7.70	13.09	ND	0.17	0.10	76.15	9.26	14.59	ND	0.19	0.12
	10 nm	77.52	8.66	13.78	0.05	0.18	0.11	76.27	9.27	13.93	0.53	0.18	0.12
	100 nm	77.85	8.66	13.49	ND	0.17	0.11	76.93	9.41	13.63	0.03	0.18	0.12

[a]Cp: pristine control. Ct: processes control. ND: not detected. Peak area ± standard deviation and relative sensitivity factors (RSF) are reported in Table S4 in the Supporting Information. The detection limits were estimated using the Shard's method as 0.01 At %.

conditions applied for hospital clothing.[18] All antibacterial data represent mean values ± SD (n = 3).

3. RESULTS AND DISCUSSION

3.1. FTIR-ATR Analysis. The FTIR-ATR spectrum of untreated PA66 (Figure 1) showed the inherent band of nylon at 3290 cm^{-1} attributed to N−H stretching vibrations. The peaks at 2920 and 2850 cm^{-1} are related to the CH_2 asymmetric and symmetric stretching vibrations, respectively, whereas the absorption band at 1630 cm^{-1} was assigned to the amide carbonyl C═O stretching vibration of the secondary amide band (amide I).[19] The amide II band at 1540 cm^{-1} may be attributed to the N−H bending motion and the band at 680 cm^{-1} to the bending of the O═C−N group.[20] After plasma treatment, significant increases in the intensity and broadening of the C═O stretching band (as well as of the bending of the O═C−N group) were observed. This is a clear indication of the microenvironmental changes and oxygen addition to the fiber surface. However, the significantly increased intensities for the N−H and both the asymmetric and the symmetric C−H stretching vibration bands at 3290, 2920, and 2850 cm^{-1}, respectively, could be attributed to the formation of low-molecular-weight etched material due to the air DBD treatment of the PA66 fabric.[21] According to the literature, ion bombardment (N_2^+, N^+, O_2^+, H_2O^+, O_2^-, and O^-) induced by plasma discharge using atmospheric air could cause the breaking of bonds with energy lower than 10 eV in the outer layers of the PA66 polymer, especially on the C−N bonds (which is the weakest bond in the polymer chain).[22] The new peak at 1740 cm^{-1}, adjacent to the increased amide C═O band at 1630 cm^{-1}, can be attributed to the C═O stretching of ketones, aldehydes, and carboxylic acids formed by air DBD treatment. The intensification of the characteristic IR peaks for $-CH_3$ (1380 cm^{-1}) and the appearance of the peak for the $-CH_2$ bend (1470 cm^{-1}) and the CH in-plane bend (1420 cm^{-1}) also suggest the formation of hydrocarbon fragments on the plasma-treated PA66 surface.[23] The new small peaks between 1000 and 1200 cm^{-1} may be attributed to the C−O stretching of free and condensed C−OH groups.[24] Nylon-6,6 has two characteristic crystalline peaks at 930 cm^{-1} (amide axial

DOI: 10.1021/acsami.5b04340
ACS Appl. Mater. Interfaces 2015, 7, 13731−13744

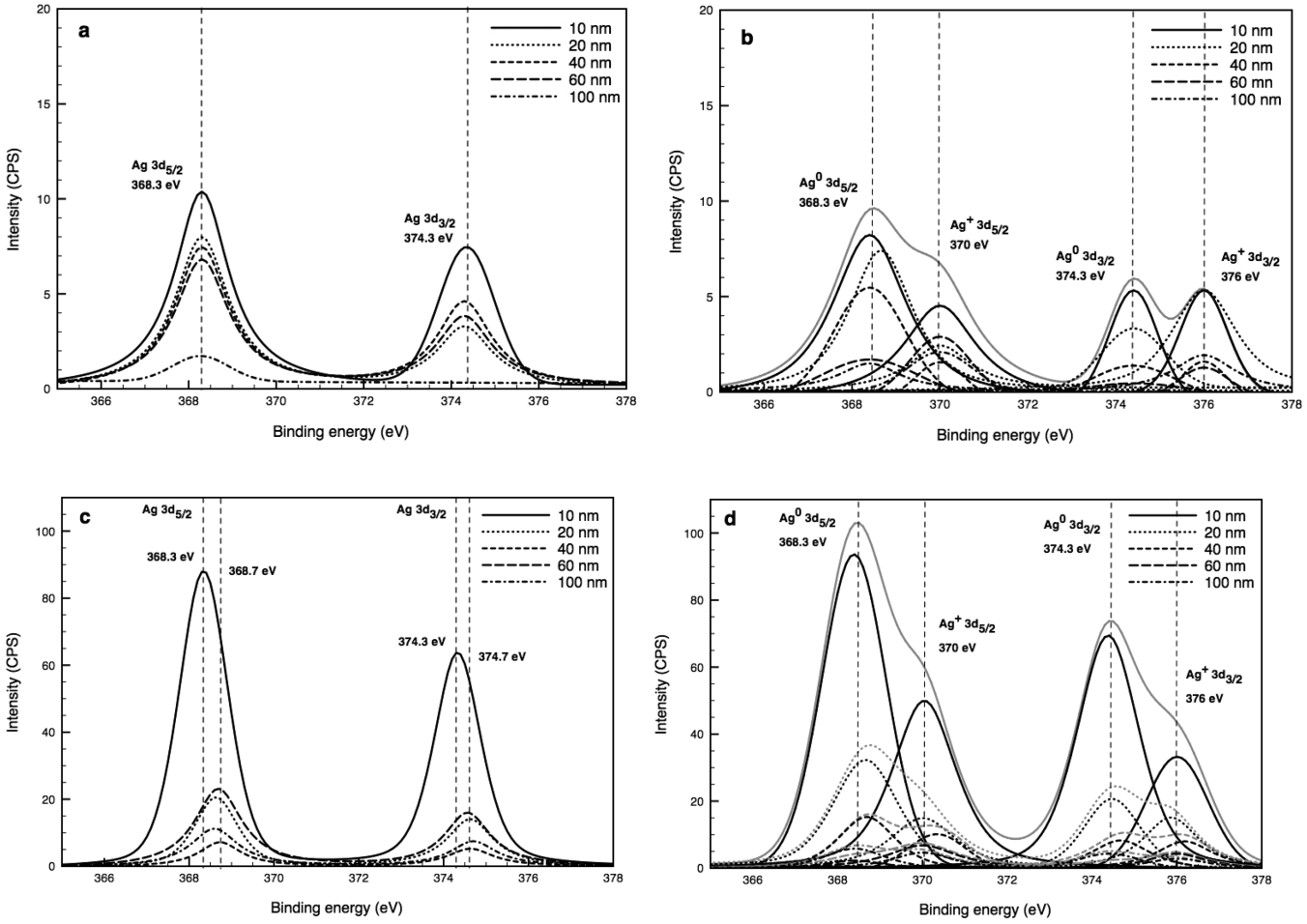

Figure 2. High-resolution deconvoluted XPS spectra of the Ag 3d binding energy region of the PA66 fiber surface before and after plasma treatment at day 1 and after 30 days. (a) Untreated, day 1. (b) Untreated, day 30. (c) Plasma-treated, day 1. (d) Plasma-treated, day 30. Fitting parameters and χ^2 error are reported in Table S4 in the Supporting Information.

deformation C−C═O) and 1200 cm^{-1} (symmetrical angular deformation out of plane, amide III). The plasma treatment changed the peak intensities in this region, indicating significant changes in crystallinity and of the C−C skeletal backbone structure.[25] Neither the nanoparticle deposition nor the 30 days of aging caused significant alterations in the infrared spectra independently on the nanoparticle sizes (data not shown). After aging 30 days, the plasma-treated surface was relatively stable and still very different from the untreated fiber. The FTIR-ATR technique, however, is not able to detect either the AgNPs on the polymer surface or changes in the noncovalent bonds such as ionic, hydrogen, van der Waals, or electrostatic forces that can significantly influence the physicochemical adhesion of the nanoparticles. Therefore, the XPS technique and diffuse reflectance spectroscopy were employed to further investigate and quantify the AgNP deposition and to elucidate the effects of the aging on the treated fabrics.

3.2. XPS Analysis. The degree of chemical modifications on the surface of the fabrics was studied by XPS (Table 1 and Table S1 in the Supporting Information). High-resolution deconvoluted XPS spectra with relative areas of the Ag 3d, C 1s, O 1s, and N 1s binding energy regions of the PA66 fiber surface before and after plasma treatment at day 1 and day 30 were also performed (Figure 2 and Table S2 and Figures S1 and S2 in the Supporting Information).

3.2.1. Relative Chemical Composition and Atomic Ratio. The relative chemical composition (C, N, O) and atomic ratios (O/C and N/C) at the surface of the untreated (without plasma activation) fabric were not significantly altered regardless of the aging process in comparison to the processed control (Ct). The pristine control (Cp) after 30 days of aging showed an increase in oxygen content, common in commercial polymers, due to low-level photo-oxidation of the central carbons of the untreated PA66.[26−28] After plasma treatment, a considerable increase in the oxygen content (especially for pristine control) and atomic O/C and N/C ratios (due to the incorporation of oxygen atoms onto the fabric surface) was observed (Table 1). Plasma etching may provoke the scission of the C−H, C−O, C−N, C−C, and N−H bonds present in the PA66 fiber, thereby promoting the formation of reactive O^-, N, N^+, O, OH^-, and O_3 species.[21,27,29] Recently, Shard (2014) has proposed an elegant approach to estimate the detection limits of XPS for any element in any elemental matrix using the intensity of the background at the expected position for the photoelectron peak to be detected. Although most elements are detectable at about the level about 1 to 0.1 At %, it is known that for heavy elements in a light element matrix, as the case in this work, the detection limit can reach 0.003 At %. This is because the detection limit is affected by not only the sensitivity factor of the trace element and the background intensity of the matrix but also the number density of atoms and the electron

DOI: 10.1021/acsami.5b04340
ACS Appl. Mater. Interfaces 2015, 7, 13731−13744

attenuation lengths in the matrix.[17] On the basis of these assumptions, the detection limits in this work were estimated using the two methods provided by Shard, displaying in both cases a value of 0.01 At %. The quantitative analyses of the Al Kα XPS spectra of the heavy element Ag 3d5/2 taken from polyamide matrix, which consists largely of light element carbon, indicate that the concentration of silver varies between 0.01 to 0.53 At %, which is in accordance with the detection limit (0.01 At %) for the untreated samples and clearly well above the detection limit for plasma-treated samples. The atomic percentage of silver remaining on the fabrics after plasma treatment was an order of magnitude higher than that for the untreated fabrics, suggesting a plasma-induced enhanced absorption of Ag. After 30 days of aging, slight increases in Ag abundance signals on the fabric surface were recorded for the smaller AgNPs (10−40 nm) on both the untreated and the plasma-treated fabrics (Table S1 in the Supporting Information). Such findings can be attributed to the morphological and chemical change of the nanoparticle microstructure due to a size-driven aging process based on a combination of nanoparticle oxidation, atomic metal diffusion, coalescence between particles, and electrochemical Ostwald ripening.[30,31]

3.2.2. Deconvolution Analysis of XPS Spectra at Day 1. XPS spectra and peak relative areas of the untreated fiber surfaces at day 1 in the region of binding energies associated with Ag 3d core electrons confirmed the presence of silver in the form of Ag^0 (Figure 2a). The energies are in good agreement with the literature values for the binding energies of silver nanoparticles.[32] The recorded very low intensities confirm the small amount of silver nanoparticles deposited on the untreated fabrics. After plasma treatment, the XPS spectra displayed a remarkable increase in the Ag peaks intensities for all of the AgNPs types, especially for 10 nm NPs (Figure 2c). This confirms the size-dependent increase in the number of dispersed AgNPs on the surface of plasma-treated PA66 fibers in comparison with that of untreated fibers. Moreover, with the exception of the 10 nm nanoparticles, all of the other AgNPs deposited on the plasma-treated PA66 fabrics showed a positive shift in the binding energy of Ag $3d_{5/2}$ (368.7 eV) relative to that of the bulk Ag (368.3 eV). This demonstrates that after the deposition of the AgNPs onto the nylon fabric, the core-shell particles reacted with the electronegative hydroxyl and carboxylic groups in the plasma-treated PA66 fibers, polarizing partially the silver nanoparticles and thus shifting to higher values the binding energy of the core electron in silver.[33,34] Moreover, it was also observed that the shift is proportional to the size of the NPs; the larger the AgNPs, the higher the binding energies are. Small NPs, associated normally to higher toxicity, bind less than larger ones. The chemical interaction between AgNPs and plasma-treated PA66 surface in the form of hydroxyl (−CO−Ag), carboxyl (−COO−Ag), or carboxylate (−COO^- Ag^+ pairs) is confirmed by the results of the deconvolution of the C 1s, O 1s, and N 1s core levels after plasma treatment (Table S2 and Figure S1 in the Supporting Information).

3.2.3. Deconvolution Analysis of XPS Spectra at Day 30. After the fabric aged for 30 days, the peaks of Ag $3d_{5/2}$ and Ag $3d_{3/2}$ became asymmetrical, and each peak can be deconvoluted into two component peaks in both the untreated and the plasma-treated fabrics (Figure 2b,d). The Ag $3d_{5/2}$ component was deconvoluted in a peak at 368.3 eV (corresponding to Ag^0) and in another peak at 370 eV, suggesting the presence of oxidized Ag that was interacting with the nylon surface.[35] Many studies indicate a negative shift in the binding energy of the Ag 3d peaks when the silver oxidation state is increased.[36,37] However, this is not the case. When silver nanoparticles or silver ions chemically interact with polymer moiety, a positive shift in binding energy with the increase in the oxidation state is usually observed, and peaks between 368.6 and 370 eV are attributed to polymer−AgO/Ag^+ ions complexes.[30,38,39] The deconvoluted C 1s, O 1s, and N 1s spectra of the plasma-treated samples after 30 days of aging returns to the same energy binding values of the untreated PA66. However, the presence of oxygen species interacting with Ag^+ ions shows a clear size effect for all NPs, and particularly for 60 and 100 nm NPs, due to their higher instability and ions release (Table S2 and Figure S2 in the Supporting Information).

3.3. Quantification of AgNPs Deposition by Diffuse Reflectance Spectroscopy. The mass concentration of the AgNPs adsorbed on the PA66 fabric was calculated by subtracting the concentration of AgNPs remaining in solution after the immobilization from the initial AgNP concentration (0.02 mg mL^{-1}). The mass concentrations of the silver nanoparticle colloids were determined according to the Lambert−Beer law from the linear relationship between the absorbance at the maximum absorption peak of each nanoparticle size versus the concentration at different dilutions (Figure 3 bottom and Figure S3 in the Supporting Information). A size-dependent deposition was observed on the plasma-treated PA66 fibers. Smaller AgNP diameters resulted in a higher mass concentration of deposited particles

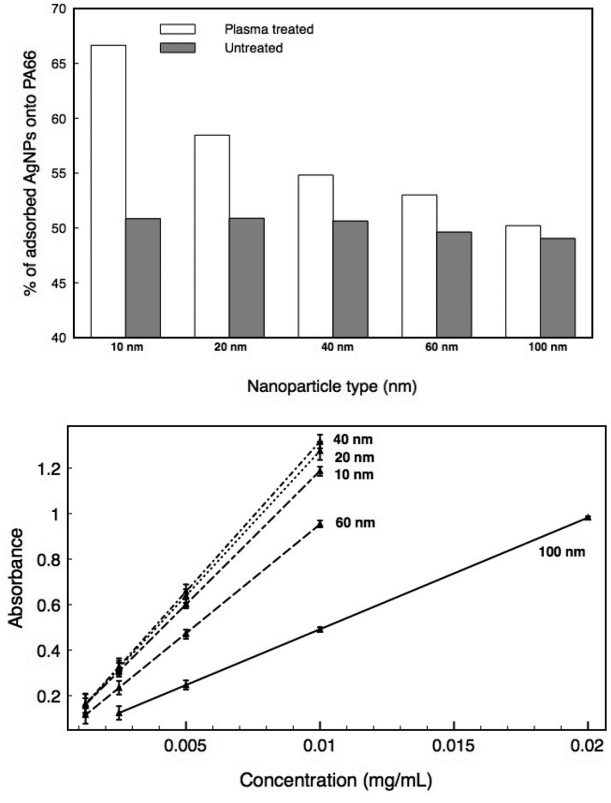

Figure 3. Percentage of the AgNPs adsorbed onto the untreated and plasma-treated PA66 (top). Linear fitting of the absorption spectra of different-sized AgNPs measured at the maximum peak absorption of the surface plasmon resonance band versus the concentration (bottom). Data represent the mean values ± SD (n = 3).

DOI: 10.1021/acsami.5b04340
ACS Appl. Mater. Interfaces 2015, 7, 13731−13744

(Figure 3). In contrast, regardless of the size of the NPs, a similar amount of adsorbed AgNPs (around 50%) was found on the nontreated PA66 fabric, probably limited to a simple physical adsorption. On the plasma-treated fabrics, a more complex deposition is expected (confirmed by the differences in the NPs' mass concentrations), which, in addition, is driven by chemical interactions with plasma-created functional groups as confirmed by the XPS analysis. At the same mass concentration, the number of the particles on the fabrics is different as a function of their size.

The influence of the loading of colloidal AgNPs onto the PA66 fabric surface before and after plasma treatment was also evaluated by diffuse reflection spectroscopy (Figure 4). The

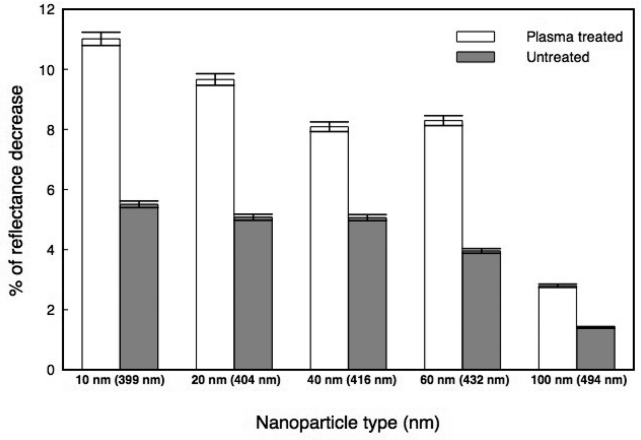

Figure 4. Percentage of the decrease in surface reflectance at maximum absorption wavelength of each different Ag nanoparticle size of untreated and plasma-treated polyamide after silver nanoparticles deposition. Data represent mean values ± SD (n = 3).

decrease in specular reflection could be considered a direct measure of the AgNPs abundance in the topmost layer of the material because the NPs act as radiation absorbers on the entire visible spectra.[9,40] All fabrics treated with plasma prior to the AgNPs' deposition displayed a higher decrease in reflectance as compared to that of the corresponding untreated samples, which confirms a larger number of AgNPs on the plasma-treated surfaces.

3.4. Static Contact Angle, Work of Adhesion, and Surface Free Energy. The static contact angles were measured to evaluate the wettability, the work of adhesion (W_{Adh}), and (by the Wu method) the total surface free energy (γ), dispersive component (γ^D), and polar component (γ^P) of the untreated and plasma-treated PA66 fabrics after the application of different-sized AgNPs. According to the data in Table 2 and in Table S3 in the Supporting Information, AgNPs loaded on the untreated fabrics (without plasma treatment) displayed similar θ_{water} values (approximately 130°) compared to those of the fabrics without AgNPs, even after 30 days of aging. The total surface free energy (γ), dispersive (γ^D), and polar component (γ^P) did not show any significant differences as well. These results suggest that the deposition of the AgNPs on the untreated PA66 is ruled by a simple physical adsorption.

After plasma treatment, a clear increase in surface polarity and wettability and in work of adhesion was observed, decreasing the static water contact angle from approximately 130° to approximately 85°. According to the thermodynamic theory, an increase in work of adhesion is indicative of an improved antibacterial activity because of the unfavorable bacterial adhesion.[41] Although the inclusion of AgNPs resulted in a decrease of θ_{water}, the NPs size was not a significant factor influencing the wettability of fabrics. Usually, with an increase in nanoparticle size, the specific surface area and free energy decrease, which should lead to an increase in the contact angle.[9,42] However, several other factors such as surface charge, roughness, and nanoparticle distribution and mass concentration control the contact angle on a fibrous material surface.[43]

In contrast to the contact angle, the surface free energy of the plasma-treated PA66 exhibited a certain dependency on the size of the deposited AgNPs. The values of the total surface free energy doubled after plasma activation (from approximately 10 to approximately 20 mJ m^{-2}). In addition, the values were slightly higher for AgNPs that were bigger in size (increasing from approximately 20 mJ m^{-2} for 10 nm AgNPs to approximately 24 mJ m^{-2} for 100 nm AgNPs). Thus, the higher the amount of AgNPs on the fabric surface, the lower the total surface free energy is. These differences can be attributed solely to the polar component because of the reorientation of the polar groups toward the fiber surface.[44] The higher values of the polar components after the deposition of the 40, 60, and 100 nm AgNPs (approximately 18 mJ m^{-2}) means that more plasma-generated oxygen species are present on the fabric surface due to the reduced amount of the loaded larger particles. Nevertheless, bigger NPs, despite their lower concentrations on the surfaces, seem to favor the electrostatic stabilization of the plasma-formed functional groups, probably due to their intrinsic instability with more Ag^+ on their

Table 2. Static Contact Angles, Surface Free Energy, and Adhesion Work in Function of Nanoparticle Size at Day 1 and After 30 Days[a]

		untreated					plasma-treated				
		θ_{water}	γ	γ^D	γ^P	W_{Adh}	θ_{water}	γ	γ^D	γ^P	W_{Adh}
day 1	Cp	119.1 ± 5.6	10.5	10.0	0.5	37.4	59.3 ± 4.9	43.4	0.5	42.9	110.0
	Ct	129.5 ± 3.4	10.5	10.0	0.5	26.5	86.3 ± 3.9	20.7	9.2	11.5	77.5
	10 nm	133.0 ± 5.5	10.5	10.0	0.5	23.2	84.0 ± 2.7	20.6	6.5	14.0	80.4
	100 nm	130.9 ± 2.7	10.5	10.0	0.5	25.1	79.3 ± 5.5	24.1	6.1	18.0	86.3
day 30	Cp	119.3 ± 4.8	10.5	10.0	0.5	37.2	81.3 ± 3.6	21.5	4.6	18.9	83.8
	Ct	130.4 ± 1.1	10.5	10.0	0.5	25.6	86.6 ± 3.3	20.3	10.4	9.8	77.1
	10 nm	129.1 ± 4.2	10.5	10.0	0.5	26.9	88.1 ± 5.8	19.6	9.8	9.9	75.2
	100 nm	130.1 ± 1.3	10.5	10.0	0.5	25.9	82.7 ± 6.4	22.1	8.7	13.4	82.1

[a]Cp: pristine control. Ct: processed control. θ_{water}: water contact angle. γ: total surface free energy. γ^D: surface free energy dispersive component. γ^P: surface free energy polar component. W_{Adh}: adhesion work. Data represent mean values ± SD (n = 5).

DOI: 10.1021/acsami.5b04340
ACS Appl. Mater. Interfaces 2015, 7, 13731−13744

surfaces.[9] The dispersive components, instead, remain constant independent of the size and number of the nanoparticles (approximately 6 mJ m^{-2}). The dispersive components of the AgNP-loaded fabrics are also significantly lower than those of the untreated (approximately 10 mJ m^{-2}) and the plasma-treated controls (9.2 mJ m^{-2}). This result indicates that the intermolecular forces acting at the interface between nanoparticles and PA66 are not dominated by London dispersive forces but by dipole−dipole interactions or hydrogen bonds.

To study the aging effect, we carried out the same measurements 30 days after the plasma pretreatment and NP deposition. It is well-known that one of the major drawbacks of plasma treatment with nonpolymerizing gases is the aging effect. During several weeks after the treatment, migration and reorientation of the oxidized groups occur, leading to a decrease in wettability and a loss of surface oxidation.[26,45] Although the storage conditions and the sample handling can slow down the process, the polymer surface dynamic appears to be the major factor in aging. The active sites on the surface undergo postreactions and restructuration due to the tendency of the polymer to achieve an energetically favorable state. The reorientation of the polar groups toward the bulk phase of the polymer hides these from the surface, exposing new unmodified fibers.[46] In our case, one month after the treatment, the PA66 contact angle and total surface free energy were similar to day 1. Such durability was achieved by storing the samples in a low relative humidity and constant temperature conditions. Despite the similar total free energy, significant differences were detected in the distribution of the dispersive and polar components as well as in the work of adhesion. The decrease of the work of adhesion and polar component and the increase of the dispersive surface energy after 30 days of aging of the AgNPs-containing plasma-activated fabrics suggest changes in the particles adhesion mechanism. The migration of hydroxyl and carboxyl groups into the bulk and the destabilization of AgNPs with the subsequent release of Ag^+ ions from the fabric's surface might have caused such changes.[47] However, due to the surface roughness and surface energy gradients of fibrous materials, the London dispersive component obtained from classical contact angle measurements can lead to unrealistic results, particularly those concerning acid−base characteristics of the surface of the analyzed material.[48] Moreover, the correlation between surface charge and adhesion is not straightforward, and this decrease appears to have no influence in the antimicrobial performance of the silver-coated aged PA66 surface (see section 3.7).[49]

3.5. Dynamic Contact Angle. Although the values of the static contact angle after plasma treatment remained relatively high, the dynamic contact angles at day 1 and after 30 days of aging showed significant deviations.

3.5.1. Dynamic Contact Angle on Untreated PA66. Without the AgNPs, the nonactivated fabrics at day 1 required more than 1 min to decrease the contact angle below 80° (Figure 5). Coating the fabric with AgNPs enhanced the hydrophilicity of the fabric in a size-dependent manner. Fabric wettability was more pronounced for larger nanoparticles; the 100 nm NP-coated fabrics required less than 10 s to decrease the contact angle below 80°, whereas the fabrics with 10 nm NP coatings required 45 s. The size effect is considerable when taking into account that the number of 100 nm NPs is much lower in comparison to the number of 10 and 20 nm NPs, and that no strong electrostatic effects rule the adhesion of the NPs on the untreated fabrics. These contradictory results confirm

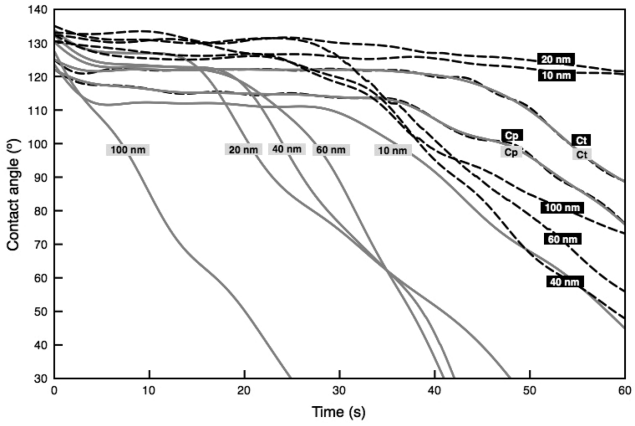

Figure 5. Dynamic contact angles of untreated fabrics at day 1 (solid gray lines) and at t = 30 days (dashed black lines) of the pristine control (Cp), the processed control (Ct), and fabrics with 10, 20, 40, 60, and 100 nm deposited AgNPs.

that nanostructures in randomly rough surfaces have a profound and in part unexplored effect on the wetting properties, probably due to a dual effect between the intrinsic hydrophilic nature of silver ions and nanoparticles and the existence of a mixed state in which both Wenzel and Cassie−Baxter regimes coexist.[43] Nanoparticle concentrations and orientations on the surface can have significant effects on both the surface roughness and the hydrophilicity.[50] In the Wenzel regime, only multiple hierarchical length scales of surface roughness can enhance water repellency by increasing the roughness factor. For small particles, the system is controlled by a mixed regime that allows neither a decrease nor an increase of the contact angle. However, this model cannot explain the behavior of the larger nanoparticles (100 nm). Such structures that are more aggregated than the smaller ones due to the higher polarization are intrinsically instable, tending to release larger amount of silver ions. It was previously reported that the silver ion deposition could improve the hydrophilic property of polymer surfaces.[51] This seems to be the only logical explanation of our findings, as the 100 nm nanoparticles are rather low in number to enhance the topological properties of the untreated PA66 surface.

After 30 days of aging, the smallest nanoparticles deposited on the untreated fabrics showed the highest increase in hydrophobicity, maintaining a contact angle of 125° after 1 min. This behavior, as previously stated, is probably due to a transition from the Wenzel regime to the Cassie−Baxter regime due to the formation of aggregates of the aged smallest nanoparticles promoting roughness effects.[52] All other (larger) nanoparticles showed similar values, maintaining a relatively high wettability with a contact angle lower than 80° after 1 min. This confirms that larger NPs are too low in number to promote roughness, and that their behavior is ruled by the release of hydrophilic silver ions.

3.5.2. Dynamic Contact Angle on Plasma-Treated PA66. In contrast to nonactivated fabrics, all plasma-treated samples at day 1 showed a significant contact angle reduction (below 10°) in less than 2 s (Figure 6). As shown above, plasma induces substantial chemical and morphological changes on the fiber surface, introducing single-bonded oxygen atoms and altering the surface topology by etching in the form of ripple-like structures of submicron size. Such modifications positively affect the loading of AgNPs of all sizes onto polymeric

DOI: 10.1021/acsami.5b04340
ACS Appl. Mater. Interfaces 2015, 7, 13731−13744

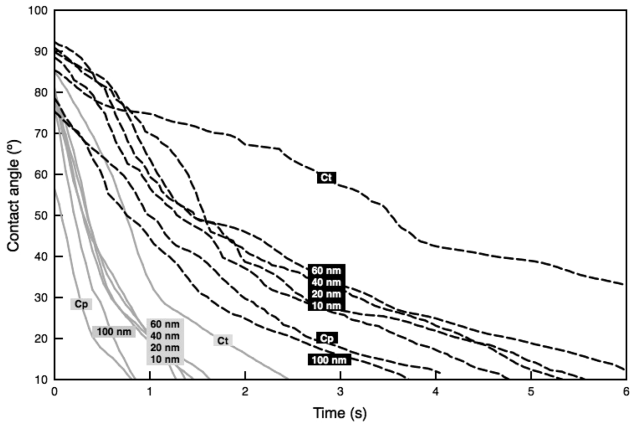

Figure 6. Dynamic contact angle of plasma-treated polyamide fabrics at day 1 (solid gray lines) and at t = 30 days (dashed black lines) of the pristine control (Cp), processed control (Ct), and fabrics with 10, 20, 40, 60, and 100 nm deposited AgNPs.

substrates. In our case, the plasma-treated PA66 fabric coated with AgNPs showed, at a different scale, the same size-dependent behavior previously observed for the untreated fabrics. The 100 nm nanoparticles showed the highest hydrophilicity, and the treated control showed the lowest hydrophilicity. The effect of aging on plasma-treated fabrics was the fastest for the samples without AgNPs. On the contrary, the PA66 fabrics loaded with AgNPs preserved, in different extents, their hydrophilicity, especially the one loaded with 100 nm nanoparticles due to the higher amount of Ag^+ on their surfaces. Once again, in agreement with the XPS and surface energy measurements, these results demonstrate the predominant role of silver ions in the electrostatic stabilization of the plasma-formed functional groups on the PA66 surface.

3.6. SEM and EDS. SEM images of untreated and plasma-treated PA66 fibers show that the topography of the fiber was uniformly altered after plasma treatment in the form of ripple-like structures of submicron size that were induced by plasma etching (Figure 7). These results are in agreement with the

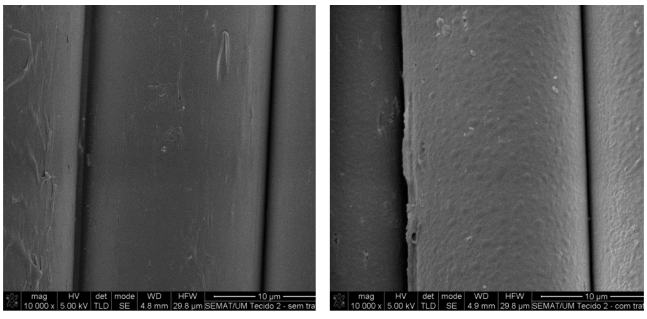

Figure 7. SEM images of untreated (left) and plasma-treated (right) PA66 fibers with a dosage of 2.5 kW min m^{-2} with a magnification of 10 000×.

literature on the effects achieved by DBD atmospheric pressure plasma treatment on synthetic fibers.[9] Energetic and highly reactive plasma species attacked the fiber surface, promoting fiber ablation and inducing an increase of the fiber surface roughness and hydrophilicity-dependent properties.

The SEM images of the five different-sized AgNPs (10, 20, 40, 60, and 100 nm) loaded in plasma-treated PA66 are characterized by a high load and widespread (but not uniform) distribution of AgNPs at the expected size range on the surface (Figure 8). However, as previously observed by Radetic et al.,[53] at this relatively low concentration (approximately 10 mg L^{-1}) and the pH used, the AgNPs stabilized in citrate buffer tend to aggregate in clusters on the surface of the DBD-treated PA66 fibers due to the thermomigration of the nanoparticles during the curing and to the surface chemical changes induced by plasma treatment.[54] The AgNP agglomerates observed on the fiber surface display a relatively constant average diameter of 100 nm, as previously also observed for similar experimental conditions.[55] All the samples contained a small quantity of AgCl crystals in the micrometric range (1−2 μm), probably generated during the synthesis of the commercial nanoparticles (Figure 8, left column). Usually, EDS is not able to establish the chemical identity of the observed nanoparticles on the PA66 surface due the deep probe depth of the technique. Nevertheless, despite this limitation, a small amount of silver was detected in the EDS spectrum of the silver-loaded fibers (Figure S4 in the Supporting Information). Moreover, the EDS spectrum confirms the presence of silver and chlorine in the observed AgCl crystals in the micrometer range.

3.7. Antimicrobial Effect. It is known that AgNPs decompose quickly after immersion in water or biological medium and release ions. The degree of dissolution of AgNPs is difficult to measure and seems to be an intrinsic size- and temperature-dependent property of the particles not related to their absolute concentration.[56] AgNPs coated on a polymer surface dissolve only partially and release silver ions more slowly. The observed proportion of metal nanoparticles (Ag^0) and released silver ions (Ag^+) depends on the NPs' size on fabrics and their aging time. Because the interaction of AgNPs with bacteria in the plasma-treated fabrics is restricted to the coated fabric surface, the XPS characterization was fundamental to understanding the observed antimicrobial properties of freshly coated and aged fabrics.

3.7.1. Antimicrobial Effect of Untreated PA66−AgNPs Fabrics. The highest Gram-positive *S. aureus* inhibition for the untreated fabrics at day 1 (Figure 9) was observed for the 60 and 100 nm AgNPs (73% and 34%, respectively), and at day 30 the higher inhibition was observed for the 40 and 10 nm AgNPs (57% and 39%, respectively). This contradictory behavior could be attributed to the Ag^+ ion release from NPs in solution during the antimicrobial tests. The NPs deposited on untreated fabrics are not stabilized and display a random mobility, during which larger NPs (60 and 100 nm) are easily released in contact with the medium. These NPs start to release ions immediately after the deposition, accounting for the observed effect at day 1, whereas after 30 days of aging, the material is almost completely depleted. Smaller NPs (10, 20, and 40 nm) decompose more slowly, showing a pronounced contribution of the Ag^+ ions on the inhibition of *S. aureus* after 30 days of aging. Indeed, the dissolution of AgNPs in biological media is complex and depends on various factors such as chemical composition, NPs' surface functionalization, concentration, and temperature.[56]

However, the results for the Gram-negative *E. coli* display bacterial inhibition only for the 10 and 20 nm AgNPs (Figure 9). The 20 nm NPs showed the same inhibition at day 1 and day 30 (approximately 25%), whereas the inhibition of the 10 nm NPs increased by approximately 60% to full kill due to the age-related release of Ag^+. The fact that the larger AgNPs in the untreated fabrics are more efficient against *S. aureus* than *E. coli* is unexpected because the greater resistance of Gram-positive

DOI: 10.1021/acsami.5b04340
ACS Appl. Mater. Interfaces 2015, 7, 13731−13744

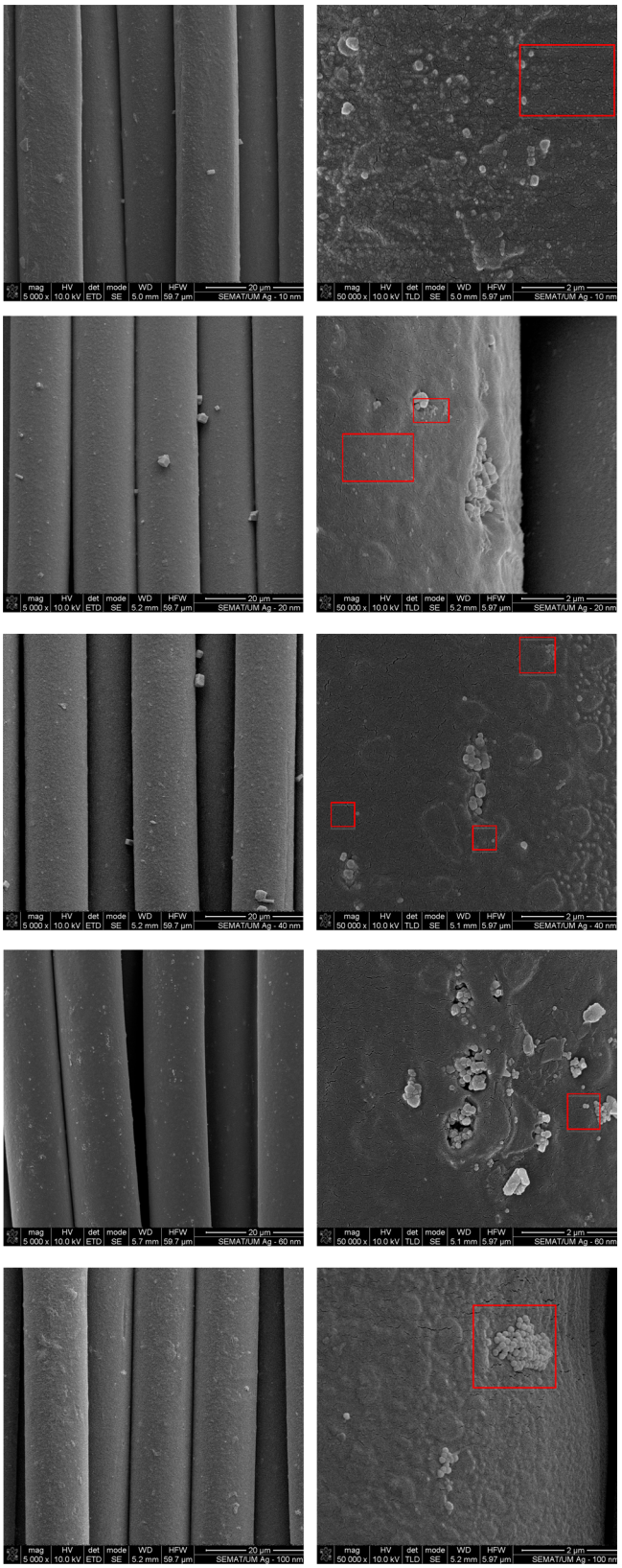

Figure 8. SEM images of plasma-treated PA66 fibers loaded with different-sized AgNPs (10, 20, 40, 60, and 100 nm in rows from top to bottom) at day 1 with a magnification of 5000× (left column) and 50 000× (right column). The nanoparticles in the inset frames are the expected size.

bacteria to silver ions is frequently reported. However, the interaction of Ag^+ ions released from AgNPs of different sizes with the thick layer of peptidoglycans in the membranes of these bacteria is still to be investigated.[57]

3.7.2. Antimicrobial Effect of Plasma-Treated PA66–AgNPs Fabrics. The results of the plasma-treated fabrics at day 1 showed a clear size-related effect: the smaller the diameter of AgNPs is, the higher the inhibition effect against *S. aureus* (from 95% for the 10 nm NPs down to 19% for the 100 nm NPs) (Figure 10). Interestingly, larger NPs were less effective in comparison to the same NPs deposited on untreated fabrics at day 1 due to the chemical bonding on the plasma-treated surface that limits their mobility, which is crucial for the immediate antibacterial effect. For the Gram-negative *E. coli*, 60 and 100 nm AgNPs also showed partial inhibitions, whereas smaller AgNPs displayed full kill (Figure 10). Due to the considerable amounts of Ag^+ released after 30 days, the growth of both the Gram-positive and the Gram-negative strains were completely inhibited by all the fabrics with the exception of the one containing 100 nm AgNPs. The reason for this could be a low amount of 100 nm NPs on the fabric surface, as was previously shown by XPS.

Although the plasma-treated fabrics coated with AgNPs displayed similar behavior for Gram-positive and Gram-negative bacteria, the variability in the inhibition extent may be explained by keeping in mind the differences in the cell wall structure and composition. The cell wall of Gram-positive bacteria is composed of a thick peptidoglycan layer consisting of linear polysaccharide chains cross-linked by short peptides to form a three-dimensional rigid structure. This rigid layer makes it difficult for the larger AgNPs to penetrate. In contrast, the cell wall of a Gram-negative species is more structurally and chemically complex because the peptidoglycan layer is thin and adjacent to the cytoplasmic membrane, while it is also constituted of a lipopolysaccharidic outer membrane. This membrane lacks strength and rigidity and is prone to the penetration by both smaller and larger AgNPs,[58] which is in accordance with our findings. In all cases, three different mechanisms of the bactericidal action of silver nanoparticles are proposed: (i) the attachment of AgNPs to the surface of the cell membrane to disturb its permeability (which is size-dependent and favors smaller NPs with high surface-to-volume ratios), (ii) the penetration of AgNPs inside the bacteria to interact with proteins and DNA due to the high affinity of silver for sulfur or phosphorus (also size-dependent in favor of smaller NPs), and (iii) the release of antibacterial silver ions. Concerning our AgNPs coated on plasma-treated fabrics, some particles are certainly released during the incubation with bacteria; however, most of the AgNPs remain attached to the fabric surface, limiting the possible penetration in the cells. Moreover, recent reports showed that the direct penetration of the microbial cell membrane was only observed for particles with sizes between 1 and 10 nm,[6] and Ag^+ has been proposed as the definitive bacterial toxicant.[59] Thus, the release of Ag^+ ions and the Ag^+/Ag^0 ratio, as functions of the NPs' size and aging time, are responsible for the antimicrobial efficiency of the AgNPs deposited on our plasma-treated PA66. After the fabric aged for 30 days, the antimicrobial effect is clearly related to the release of silver ions independent of the size and number of the AgNPs up to 60 nm. Because the nanoparticles larger than 30 nm have been reported not to induce nanotoxicity in human cells (in contrast to the effect of smaller particles), the use of the latter in the surface coatings of materials in direct

DOI: 10.1021/acsami.5b04340
ACS Appl. Mater. Interfaces 2015, 7, 13731−13744

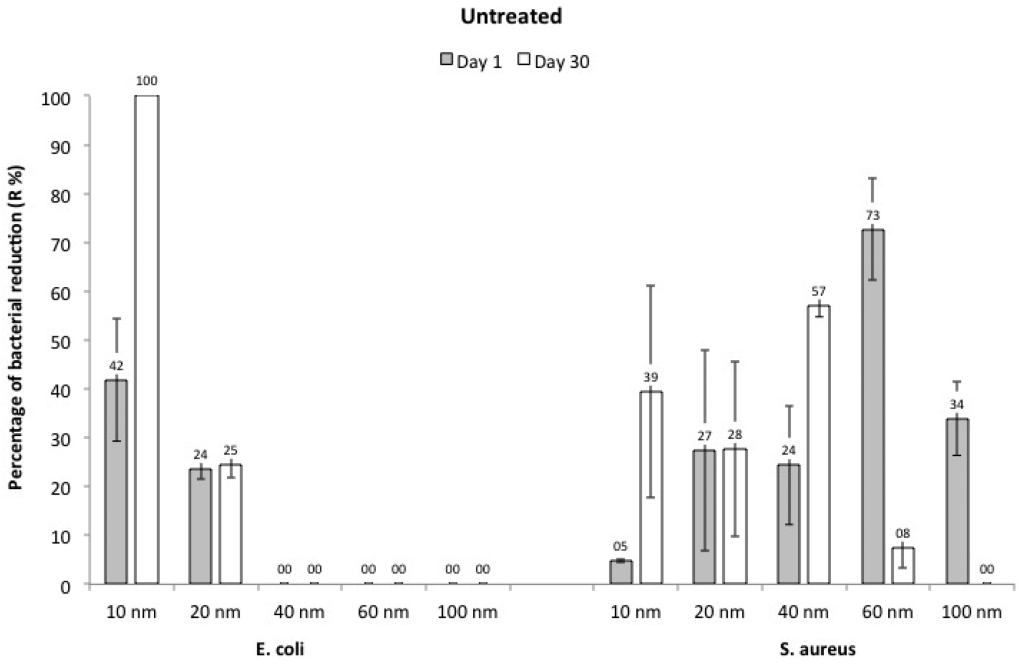

Figure 9. *Escherichia coli* and *Staphylococcus aureus* growth reduction with respect to the control fabric of untreated PA66 loaded with different-sized AgNPs at day 1 and after 30 days.

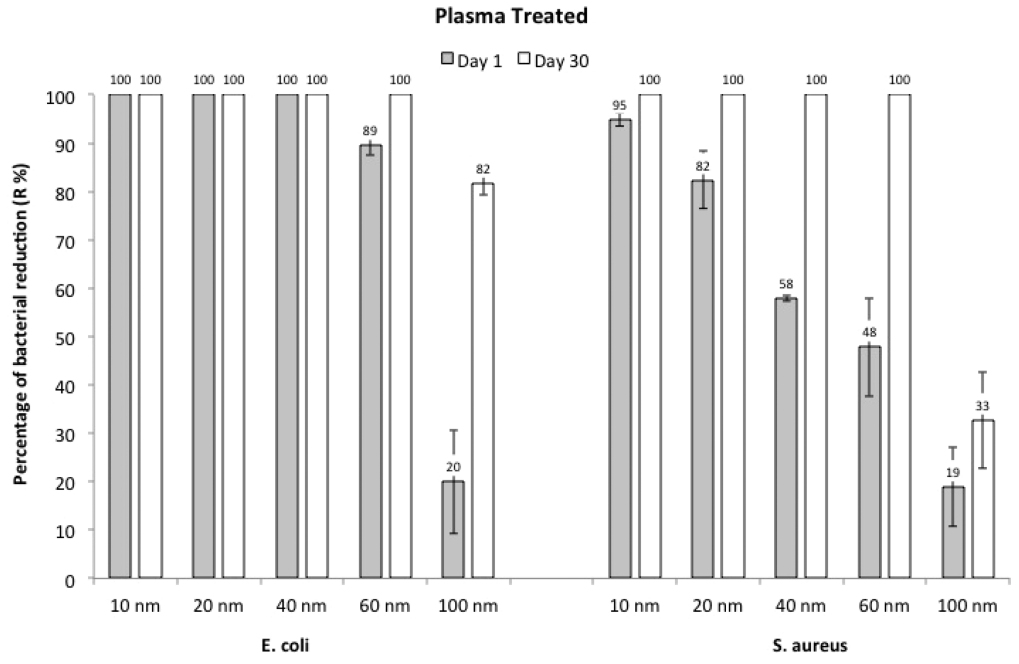

Figure 10. *E, coli* and *S. aureus* growth reduction with respect to the control fabric of plasma-treated PA66 loaded with different-sized AgNPs at day 1 and after 30 days.

contact with humans should be avoided.[15] However, the 100 nm AgNPs did not achieve the antimicrobial performance comparable to the ones obtained with the AgNPs of smaller size. One advantage of using AgNPs instead of silver salts on textiles relies on the fact that nanoparticles allow for a sustained release of Ag^+ ions due to the size-related Ag^+/Ag^0 ratio on their surface,[60] which, as in our case, permits using lower concentrations that induce sufficient antibacterial activity. Both thermodynamic and experimental data suggest that AgNPs are converted to ions by a slow reactive dissolution (6−125 days) that allows a higher control release of silver ions than do silver salts at the same local concentrations,[61,62] which is crucial to achieve the desired properties of hospital textiles.[63,64]

3.7.3. Durability of Antimicrobial Properties. Because hospital clothing is frequently washed to minimize the transfer of pathogens, our fabrics were evaluated for the durability of the antimicrobial effect after applying up to 20 high-temperature washings. Due to the large number of samples and to simplify the discussion, the evaluation was carried out only for the nonaged PA66 (untreated and plasma treated) loaded with 40

DOI: 10.1021/acsami.5b04340
ACS Appl. Mater. Interfaces 2015, 7, 13731−13744

nm AgNPs. These fabrics were selected for testing the durability of the effect as sufficiently effective in terms of their antimicrobial activity for at least one bacterial strain (*S. aureus*, evaluated in this study) and safety (due to their size and our reliance on the literature data). Because the untreated fabric loaded with 40 nm particles did not show a bactericidal effect toward *E. coli*, the results comment solely on the *S. aureus* growth inhibition. In the case of the latter, the AgNP-loaded fabric had already lost more than half of its antibacterial activity after the first washing, and a negligible effect is detected already after 5 washings (Table 3). In contrast, pretreatment of the fabrics with plasma resulted in a more durable antibacterial effect of the loaded AgNPs for both *E. coli* and *S. aureus*. When calculated, more than 90% of the effect was preserved after 20 washings in the case of *E. coli*, whereas it dropped to approximately 80% for *S. aureus*, which could be considered as an acceptable loss.[65]

Table 3. Percentage of Inhibition of *E. coli* and *S. aureus* Growth on PA66 Loaded with 40 nm AgNPs After Different Numbers of Washings

	untreated		plasma-treated	
washing cycles	*E. coli*	*S. aureus*	*E. coli*	*S. aureus*
0	0	24.5 ± 4.2	100	55.7 ± 8.4
1	0	9.3 ± 3.8	100	55.3 ± 7.4
5	0	1.7 ± 0.7	98.9 ± 1.4	54.0 ± 5.6
10	0	0	92.3 ± 8.2	45.6 ± 5.2
20	0	0	91.7 ± 9.0	46.4 ± 2.9

Because the loading of untreated PA66 fabrics is limited to the physical adsorption of AgNPs, the progressive antibacterial activity loss due to washings indicates that the effect lasted until the particles (which are easily removed by washings) persisted on the fabric surface. However, the plasma-pretreated fabrics preserved most of the antibacterial effect after the washings, and the slightly lower effects could be explained by the release of a smaller portion of AgNPs physically adsorbed on the surface. Similar conclusions could be drawn from the materials with covalently grafted AgNPs via auxiliary macromolecules, e.g., biopolymers.[66] It is therefore the plasma pretreatment that, besides the improved inhibition of bacteria growth, brings about the washing stability and durability to the antimicrobial fabrics. The understanding of how particular technological processes (e.g., plasma pretreatment) and aging influence the efficiency and stability of the antimicrobial textiles may lead to substantial contributions to the standardization in production of durable antibacterial clothing and textiles, making clinical settings safer places.[67]

4. CONCLUSIONS

Plasma treatment induces substantial morphological and physicochemical changes onto the PA66 fiber's surface, enhancing its roughness, surface energy, and wettability and consequently improving AgNP adhesion. This work demonstrates the complexity of the ionic and the covalent interactions between AgNPs and the plasma-generated electronegative oxygen groups on the PA66 surface that strongly depend on the NPs' size. In contrast, the functionalization of untreated PA66 fabrics is limited to a simple physical adsorption and depends only on the AgNPs number but not on their size. After aging for 30 days, both the untreated and the plasma-treated fabrics showed a gradual release of Ag^+ ions from AgNPs. The Ag^+ release favors the electrostatic stabilization of the functional groups induced by the plasma treatment retarding their migration into the polymer bulk and ultimately contributing to the durability of the plasma-assisted coatings. Such interactions influenced to a large extent the antibacterial properties of the treated fabrics. The inhibition of bacterial growth at day 1 is clearly driven by the number and size of the AgNPs and improved with the decrease in the AgNPs' diameter. However, after 30 days of aging, the fabrics functionalized with larger AgNPs (with the exception of 100 nm particles) showed comparable inhibition effects to those treated with 10 and 20 nm AgNPs.

Overall, the use of the cytotoxic small nanoparticles (10−20 nm) for the coating of polymeric materials can be avoided because the increased bactericidal effect of AgNPs is mainly ruled by the release of Ag^+ over time and not by the size and number of the nanoparticles. Likewise, it demonstrates the advantage of using 40−60 nm AgNPs due to their capability for sustained release of Ag^+ ions sufficient to achieve the antibacterial effect at lower concentrations than those of bulk silver. From a technological point of view, aside from the absence of toxicity issues, the use of AgNPs larger than 30 nm would also avoid additional efforts toward the synthesis and stabilization of smaller particles.

■ ASSOCIATED CONTENT

Supporting Information

Additional discussion about the deconvolution analysis of XPS including figures and tables of high-resolution deconvoluted XPS spectra, relative chemical composition, and atomic ratio. Supplementary table data for static contact angles, surface free energy, adhesion work, standard deviations, Relative Sensitivity Factors, χ^2 values, and full width half maximum and Gauss−Lorentz mixing ratio of XPS data. Figure and discussion of UV−visible spectrophotometric analysis and the EDS spectra of DBD plasma-treated PA66 fabrics at day 1 with 10 nm AgNPs. The Supporting Information is available free of charge on the ACS Publications website at DOI: 10.1021/acsami.5b04340.

■ AUTHOR INFORMATION

Corresponding Author

*E-mail: azille@2c2t.uminho.pt, andrea.zille@gmail.com.

Author Contributions

The manuscript was written through contributions of all authors. All authors have given approval to the final version of the manuscript.

Funding

This work is supported by Portuguese National Funding, through FCT - Fundação para a Ciência e a Tecnologia, on the framework of project UID/CTM/00264/2013.

Notes

The authors declare no competing financial interest.

■ ACKNOWLEDGMENTS

A.Z. (C2011-UMINHO-2C2T-01) acknowledges FCT funding from Programa Compromisso para a Ciência 2008, Portugal. F.O. (SFRH/BD/65254/2009) acknowledges Fundação para a Ciência e Tecnologia (FCT), Portugal, for his doctoral grant financial support. XPS studies were performed at CEMUP (University of Porto, Portugal) facilities.

DOI: 10.1021/acsami.5b04340
ACS Appl. Mater. Interfaces 2015, 7, 13731−13744

REFERENCES

(1) Rai, M.; Yadav, A.; Gade, A. Silver Nanoparticles as a New Generation of Antimicrobials. *Biotechnol. Adv.* **2009**, *27*, 76−83.

(2) Chopra, I. The Increasing Use of Silver-Based Products as Antimicrobial Agents: A Useful Development or a Cause for Concern? *J. Antimicrob. Chemother.* **2007**, *59*, 587−590.

(3) Fonder, M. A.; Lazarus, G. S.; Cowan, D. A.; Aronson-Cook, B.; Kohli, A. R.; Mamelak, A. J. Treating the Chronic Wound: A Practical Approach to the Care of Nonhealing Wounds and Wound Care Dressings. *J. Am. Acad. Dermatol.* **2008**, *58*, 185−206.

(4) Dastjerdi, R.; Montazer, M. A Review on the Application of Inorganic Nano-Structured Materials in the Modification of Textiles: Focus on Anti-Microbial Properties. *Colloids Surf., B* **2010**, *79*, 5−18.

(5) Chernousova, S.; Epple, M. Silver as Antibacterial Agent: Ion, Nanoparticle, and Metal. *Angew. Chem., Int. Ed.* **2013**, *52*, 1636−1653.

(6) Emam, H. E.; Manian, A. P.; Široká, B.; Duelli, H.; Redl, B.; Pipal, A.; Bechtold, T. Treatments to Impart Antimicrobial Activity to Clothing and Household Cellulosic Textiles − Why "Nano"-Silver? *J. Cleaner Prod.* **2013**, *39*, 17−23.

(7) Shahid-ul-Islam; Shahid, M.; Mohammad, F. Green Chemistry Approaches to Develop Antimicrobial Textiles Based on Sustainable Biopolymers—A Review. *Ind. Eng. Chem. Res.* **2013**, *52*, 5245−5260.

(8) Zille, A.; Oliveira, F. R.; Souto, A. P. Plasma Treatment in Textile Industry. *Plasma Processes Polym.* **2014**, *12*, 98−131.

(9) Vu, N. K.; Zille, A.; Oliveira, F. R.; Carneiro, N.; Souto, A. P. Effect of Particle Size on Silver Nanoparticle Deposition onto Dielectric Barrier Discharge (DBD) Plasma Functionalized Polyamide Fabric. *Plasma Processes Polym.* **2013**, *10*, 285−296.

(10) Takke, V.; Behary, N.; Perwuelz, A.; Campagne, C. Studies on the Atmospheric Air−Plasma Treatment of PET (Polyethylene Terephtalate) Woven Fabrics: Effect of Process Parameters and of Aging. *J. Appl. Polym. Sci.* **2009**, *114*, 348−357.

(11) Morones, J. R.; Elechiguerra, J. L.; Camacho, A.; Holt, K.; Kouri, J. B.; Ramirez, J. T.; Yacaman, M. J. The Bactericidal Effect of Silver Nanoparticles. *Nanotechnology* **2005**, *16*, 2346−2353.

(12) Liu, H. L.; Dai, S. A.; Fu, K. Y.; Hsu, S. H. Antibacterial Properties of Silver Nanoparticles in Three Different Sizes and Their Nanocomposites with a New Waterborne Polyurethane. *Int. J. Nanomed.* **2010**, *5*, 1017−1028.

(13) Pal, S.; Tak, Y. K.; Song, J. M. Does the Antibacterial Activity of Silver Nanoparticles Depend on the Shape of the Nanoparticle? A Study of the Gram-Negative Bacterium *Escherichia coli*. *Appl. Environ. Microbiol.* **2007**, *73*, 1712−1720.

(14) Marambio-Jones, C.; Hoek, E. M. V. A Review of the Antibacterial Effects of Silver Nanomaterials and Potential Implications for Human Health and the Environment. *J. Nanopart. Res.* **2010**, *12*, 1531−1551.

(15) Auffan, M.; Rose, J.; Bottero, J. Y.; Lowry, G. V.; Jolivet, J. P.; Wiesner, M. R. Towards a Definition of Inorganic Nanoparticles from an Environmental, Health, and Safety Perspective. *Nat. Nanotechnol.* **2009**, *4*, 634−641.

(16) Mark, S. S.; Bergkvist, M.; Yang, X.; Angert, E. R.; Batt, C. A. Self-Assembly of Dendrimer-Encapsulated Nanoparticle Arrays Using 2D Microbial S-Layer Protein Biotemplates. *Biomacromolecules* **2006**, *7*, 1884−1897.

(17) Shard, A. G. Detection Limits in XPS for More Than 6000 Binary Systems Using Al and Mg Kα X-Rays. *Surf. Interface Anal.* **2014**, *46*, 175−185.

(18) Petkova, P.; Francesko, A.; Fernandes, M. M.; Mendoza, E.; Perelshtein, I.; Gedanken, A.; Tzanov, T. Sonochemical Coating of Textiles with Hybrid ZnO/Chitosan Antimicrobial Nanoparticles. *ACS Appl. Mater. Interfaces* **2014**, *6*, 1164−1172.

(19) Charles, J.; Ramkumaar, G. R.; Azhagiri, S.; Gunasekaran, S. FTIR and Thermal Studies on Nylon 6,6 and 30% Glass Fibre Reinforced Nylon 6,6. *E-J. Chem.* **2009**, *6*, 23−33.

(20) Kale, K. H.; Palaskar, S. S. Structural Studies of Plasma Polymers Obtained in Pulsed Dielectric Barrier Discharge of TEOS and HDMSO on Nylon 6,6 Fabrics. *J. Text. Inst.* **2012**, *103*, 1088−1098.

(21) Upadhyay, D. J.; Cui, N. Y.; Anderson, C. A.; Brown, N. M. D. A Comparative Study of the Surface Activation of Polyamides Using an Air Dielectric Barrier Discharge. *Colloids Surf., A* **2004**, *248*, 47−56.

(22) Menchaca, C.; Alvarez-Castillo, A.; Martinez-Barrera, G.; Lopez-Valdivia, H.; Carrasco, H.; Castano, V. M. Mechanisms for the Modification of Nylon 6,12 by γ Irradiation. *Int. J. Mater. Prod. Technol.* **2003**, *19*, 521−529.

(23) Zheng, Y.; Liu, H. Y.; Gurgel, P. V.; Carbonell, R. G. Polypropylene Nonwoven Fabrics with Conformal Grafting of Poly(glycidyl methacrylate) for Bioseparations. *J. Membr. Sci.* **2010**, *364*, 362−371.

(24) Goodarzi, V.; Jafari, S. H.; Khonakdar, H. A.; Ghalei, B.; Mortazavi, M. Assessment of Role of Morphology in Gas Permselectivity of Membranes Based on Polypropylene/Ethylene Vinyl Acetate/Clay Nanocomposite. *J. Membr. Sci.* **2013**, *445*, 76−87.

(25) Navarro-Pardo, F.; Martínez-Barrera, G.; Martínez-Hernández, A.; Castaño, V.; Rivera-Armenta, J.; Medellín-Rodríguez, F.; Velasco-Santos, C. Effects on the Thermo-Mechanical and Crystallinity Properties of Nylon 6,6 Electrospun Fibres Reinforced with One Dimensional (1D) and Two Dimensional (2D) Carbon. *Materials* **2013**, *6*, 3494−3513.

(26) Borcia, G.; Dumitrascu, N.; Popa, G. Influence of Helium−Dielectric Barrier Discharge Treatments on the Adhesion Properties of Polyamide-6 Surfaces. *Surf. Coat. Technol.* **2005**, *197*, 316−321.

(27) Zhu, L.; Wang, C. X.; Qiu, Y. P. Influence of the Amount of Absorbed Moisture in Nylon Fibers on Atmospheric Pressure Plasma Processing. *Surf. Coat. Technol.* **2007**, *201*, 7453−7461.

(28) Morent, R.; De Geyter, N.; Leys, C.; Gengembre, L.; Payen, E. Surface Modification of Non-woven Textiles Using a Dielectric Barrier Discharge Operating in Air, Helium and Argon at Medium Pressure. *Text. Res. J.* **2007**, *77*, 471−488.

(29) Zhou, Q.; Wang, K.; Loo, L. S. Investigation of Surface Properties of Plasma-Modified Polyamide 6 and Polyamide 6/Layered Silicate Nanocomposites. *J. Mater. Sci.* **2010**, *46*, 3084−3093.

(30) Zanna, S.; Saulou, C.; Mercier-Bonin, M.; Despax, B.; Raynaud, P.; Seyeux, A.; Marcus, P. Ageing of Plasma-Mediated Coatings with Embedded Silver Nanoparticles on Stainless Steel: An XPS and TOF-SIMS Investigation. *Appl. Surf. Sci.* **2010**, *256*, 6499−6505.

(31) Wang, X.; Somsen, C.; Grundmeier, G. Ageing of Thin Ag/Fluorocarbon Plasma Polymer Nanocomposite Films Exposed to Water-Based Electrolytes. *Acta Mater.* **2008**, *56*, 762−773.

(32) Bowering, N.; Croston, D.; Harrison, P. G.; Walker, G. S. Silver Modified Degussa P25 for the Photocatalytic Removal of Nitric Oxide. *Int. J. Photoenergy* **2007**, *90752*, 1−8.

(33) Nischala, K.; Rao, T. N.; Hebalkar, N. Silica-Silver Core-Shell Particles for Antibacterial Textile Application. *Colloids Surf., B* **2011**, *82*, 203−208.

(34) Bootharaju, M. S.; Pradeep, T. Uptake of Toxic Metal Ions from Water by Naked and Monolayer Protected Silver Nanoparticles: An X-rRay Photoelectron Spectroscopic Investigation. *J. Phys. Chem. C* **2010**, *114*, 8328−8336.

(35) Sumesh, E.; Bootharaju, M. S.; Anshup; Pradeep, T. A Practical Silver Nanoparticle-Based Adsorbent for the Removal of Hg^{2+} from Water. *J. Hazard. Mater.* **2011**, *189*, 450−457.

(36) Liu, W.; Li, B.; Cao, R.; Jiang, Z.; Yu, S.; Liu, G.; Wu, H. Enhanced Pervaporation Performance of Poly(dimethyl siloxane) Membrane by Incorporating Titania Microspheres with High Silver Ion Loading. *J. Membr. Sci.* **2011**, *378*, 382−392.

(37) Itani, H.; Keil, P.; Lützenkirchen-Hecht, D.; Haake, U.; Bongard, H.; Dreier, A.; Lehmann, C. W.; Grundmeier, G. XANES Studies of the Formation of Ag Nanoparticles in LbL-Deposited Polyelectrolyte Thin Films. *Surf. Coat. Technol.* **2010**, *205*, 2113−2119.

(38) Liu, F.; Cao, Z.; Tang, C.; Chen, L.; Wang, Z. Ultrathin Diamond-Like Carbon Film Coated Silver Nanoparticles-Based Substrates for Surface-Enhanced Raman Spectroscopy. *ACS Nano* **2010**, *4*, 2643−2648.

(39) Davoudi, Z. M.; Kandjani, A. E.; Bhatt, A. I.; Kyratzis, I. L.; O'Mullane, A. P.; Bansal, V. Hybrid Antibacterial Fabrics with

DOI: 10.1021/acsami.5b04340
ACS Appl. Mater. Interfaces 2015, 7, 13731−13744

Extremely High Aspect Ratio Ag/AgTCNQ Nanowires. *Adv. Funct. Mater.* **2014**, *24*, 1047−1053.
(40) Montazer, M.; Shamei, A.; Alimohammadi, F. Synthesis of Nanosilver on Polyamide Fabric Using Silver/Ammonia Complex. *Mater. Sci. Eng., C* **2014**, *38*, 170−176.
(41) Marciano, F. R.; Lima-Oliveira, D. A.; Da-Silva, N. S.; Diniz, A. V.; Corat, E. J.; Trava-Airoldi, V. J. Antibacterial Activity of DLC Films Containing TiO_2 Nanoparticles. *J. Colloid Interface Sci.* **2009**, *340*, 87−92.
(42) Munshi, A. M.; Singh, V. N.; Kumar, M.; Singh, J. P. Effect of Nanoparticle Size on Sessile Droplet Contact Angle. *J. Appl. Phys.* **2008**, *103*, 084315.
(43) Li, X. M.; He, T.; Crego-Calama, M.; Reinhoudt, D. N. Conversion of a Metastable Superhydrophobic Surface to an Ultraphobic Surface. *Langmuir* **2008**, *24*, 8008−8012.
(44) Stachewicz, U.; Barber, A. H. Enhanced Wetting Behavior at Electrospun Polyamide Nanofiber Surfaces. *Langmuir* **2011**, *27*, 3024−3029.
(45) Qufu, W.; Yingying, W.; Qin, Y.; Liangyan, Y. Functionalization of Textile Materials by Plasma Enhanced Modification. *J. Ind. Text.* **2007**, *36*, 301−309.
(46) Canal, C.; Molina, R.; Bertran, E.; Erra, P. Wettability, Ageing and Recovery Process of Plasma-Treated Polyamide 6. *J. Adhes. Sci. Technol.* **2004**, *18*, 1077−1089.
(47) Ferrero, F.; Bongiovanni, R. Improving the Surface Properties of Cellophane by Air Plasma Treatment. *Surf. Coat. Technol.* **2006**, *200*, 4770−4776.
(48) Gamelas, J. A. F. The Surface Properties of Cellulose and Lignocellulosic Materials Assessed by Inverse Gas Chromatography: A Review. *Cellulose* **2013**, *20*, 2675−2693.
(49) Katsikogianni, M.; Missirlis, Y. F. Concise Review of Mechanisms of Bacterial Adhesion to Biomaterials and of Techniques Used in Estimating Bacteria-Material Interactions. *Eur. Cells Mater.* **2004**, *8*, 37−57.
(50) Dastjerdi, R.; Montazer, M.; Shahsavan, S. A Novel Technique for Producing Durable Multifunctional Textiles Using Nanocomposite Coating. *Colloids Surf., B* **2010**, *81*, 32−41.
(51) Li, J. X.; Wang, J.; Shen, L. R.; Xu, Z. J.; Li, P.; Wan, G. J.; Huang, N. The Influence of Polyethylene Terephthalate Surfaces Modified by Silver Ion Implantation on Bacterial Adhesion Behavior. *Surf. Coat. Technol.* **2007**, *201*, 8155−8159.
(52) Yüce, M. Y.; Demirel, A. L. The Effect of Nanoparticles on the Surface Hydrophobicity of Polystyrene. *Eur. Phys. J. B* **2008**, *64*, 493−497.
(53) Radetic, M.; Ilic, V.; Vodnik, V.; Dimitrijevic, S.; Jovancic, P.; Saponjic, Z.; Nedeljkovic, J. M. Antibacterial Effect of Silver Nanoparticles Deposited on Corona-Treated Polyester and Polyamide Fabrics. *Polym. Adv. Technol.* **2008**, *19*, 1816−1821.
(54) Montazer, M.; Shamei, A.; Alimohammadi, F. Stabilized Nanosilver Loaded Nylon Knitted Fabric Using BTCA without Yellowing. *Prog. Org. Coat.* **2012**, *74*, 270−276.
(55) Song, J.; Birbach, N. L.; Hinestroza, J. P. Deposition of Silver Nanoparticles on Cellulosic Fibers Via Stabilization of Carboxymethyl Groups. *Cellulose* **2012**, *19*, 411−424.
(56) Kittler, S.; Greulich, C.; Diendorf, J.; Köller, M.; Epple, M. Toxicity of Silver Nanoparticles Increases During Storage Because of Slow Dissolution under Release of Silver Ions. *Chem. Mater.* **2010**, *22*, 4548−4554.
(57) Amato, E.; Diaz-Fernandez, Y. A.; Taglietti, A.; Pallavicini, P.; Pasotti, L.; Cucca, L.; Milanese, C.; Grisoli, P.; Dacarro, C.; Fernandez-Hechavarria, J. M.; Necchi, V. Synthesis, Characterization and Antibacterial Activity against Gram Positive and Gram Negative Bacteria of Biomimetically Coated Silver Nanoparticles. *Langmuir* **2011**, *27*, 9165−9173.
(58) Hajipour, M. J.; Fromm, K. M.; Akbar Ashkarran, A.; Jimenez de Aberasturi, D.; Larramendi, I. R. d.; Rojo, T.; Serpooshan, V.; Parak, W. J.; Mahmoudi, M. Antibacterial Properties of Nanoparticles. *Trends Biotechnol.* **2012**, *30*, 499−511.
(59) Xiu, Z.-m.; Zhang, Q.-b.; Puppala, H. L.; Colvin, V. L.; Alvarez, P. J. J. Negligible Particle-Specific Antibacterial Activity of Silver Nanoparticles. *Nano Lett.* **2012**, *12*, 4271−4275.
(60) Chaloupka, K.; Malam, Y.; Seifalian, A. M. Nanosilver as a New Generation of Nanoproduct in Biomedical Applications. *Trends Biotechnol.* **2010**, *28*, 580−588.
(61) Reidy, B.; Haase, A.; Luch, A.; Dawson, K.; Lynch, I. Mechanisms of Silver Nanoparticle Release, Transformation and Toxicity: A Critical Review of Current Knowledge and Recommendations for Future Studies and Applications. *Materials* **2013**, *6*, 2295−2350.
(62) Damm, C.; Münstedt, H. Kinetic Aspects of the Silver Ion Release from Antimicrobial Polyamide/Silver Nanocomposites. *Appl. Phys. A: Mater. Sci. Process.* **2008**, *91*, 479−486.
(63) Kim, J. S.; Kuk, E.; Yu, K. N.; Kim, J.-H.; Park, S. J.; Lee, H. J.; Kim, S. H.; Park, Y. K.; Park, Y. H.; Hwang, C.-Y.; Kim, Y.-K.; Lee, Y.-S.; Jeong, D. H.; Cho, M.-H. Antimicrobial Effects of Silver Nanoparticles. *Nanomed. Nanotechnol. Biol. Med.* **2007**, *3*, 95−101.
(64) Knetsch, M. L. W.; Koole, L. H. New Strategies in the Development of Antimicrobial Coatings: The Example of Increasing Usage of Silver and Silver Nanoparticles. *Polymers* **2011**, *3*, 340−366.
(65) Perelshtein, I.; Ruderman, Y.; Perkas, N.; Traeger, K.; Tzanov, T.; Beddow, J.; Joyce, E.; Mason, T. J.; Blanes, M.; Mollá, K.; Gedanken, A. Enzymatic Pre-Treatment as a Means of Enhancing the Antibacterial Activity and Stability of ZnO Nanoparticles Sonochemically Coated on Cotton Fabrics. *J. Mater. Chem.* **2012**, *22*, 10736.
(66) Francesko, A.; Blandón, L.; Vázquez, M.; Petkova, P.; Morató, J.; Pfeifer, A.; Heinze, T.; Mendoza, E.; Tzanov, T. Enzymatic Functionalization of Cork Surface with Antimicrobial Hybrid Biopolymer/Silver Nanoparticles. *ACS Appl. Mater. Interfaces* **2015**, *7*, 9792−9799.
(67) Perelshtein, I.; Lipovsky, A.; Perkas, N.; Tzanov, T.; Arguirova, M.; Leseva, M.; Gedanken, A. Making the Hospital a Safer Place by Sonochemical Coating of All Its Textiles with Antibacterial Nanoparticles. *Ultrason. Sonochem.* **2015**, *25*, 82−88.

DOI: 10.1021/acsami.5b04340
ACS Appl. Mater. Interfaces 2015, 7, 13731−13744